Benchmarking of novel green fluorescent proteins for the quantification of protein oligomerization in living cells

Annett Petrich[1], Amit Koikkarah Aji[1], Valentin Dunsing[1,2], Salvatore Chiantia[1,‡]

[1] University of Potsdam, Institute of Biochemistry and Biology, Karl-Liebknecht-Straße 24-25, 14476 Potsdam, Germany

[2] Aix-Marseille University, CNRS, UMR 7288, IBDM, Turing Center for Living Systems, Marseille, France

[‡] Correspondence: chiantia@uni-potsdam.de

Short title: Benchmarking of green fluorescent proteins via sFCS and N&B

Abstract

Protein-protein-interactions play an important role in several cellular functions. Quantitative non-invasive techniques are applied in living cells to evaluate such interactions, thereby providing a broader understanding of complex biological processes. Fluorescence fluctuation spectroscopy describes a group of quantitative microscopy approaches for the characterization of molecular interactions at single cell resolution. Through the obtained molecular brightness, it is possible to determine the oligomeric state of proteins. This is usually achieved by fusing fluorescent proteins (FPs) to the protein of interest. Recently, the number of novel green FPs has increased, with consequent improvements to the quality of fluctuation-based measurements. The photophysical behavior of FPs is influenced by multiple factors (including photobleaching, protonation-induced "blinking" and long-lived dark states). Assessing these factors is critical for selecting the appropriate fluorescent tag for live cell imaging applications. In this work, we focus on novel green FPs that are extensively used in live cell imaging. A systematic performance comparison of several green FPs in living cells under different pH conditions using Number & Brightness

(N&B) analysis and scanning fluorescence correlation spectroscopy was performed. Our results show that the new FP Gamillus exhibits higher brightness at the cost of lower photostability and fluorescence probability (*pf*), especially at lower pH. mGreenLantern, on the other hand, thanks to a very high *pf*, is best suited for multimerization quantification at neutral pH. At lower pH, mEGFP remains apparently the best choice for multimerization investigation. These guidelines provide the information needed to plan quantitative fluorescence microscopy involving these FPs, both for general imaging or for Protein-protein-interactions quantification via fluorescence fluctuation-based methods.

Keywords

Fluorescence correlation spectroscopy, fluorescence microscopy, fluorescence fluctuation spectroscopy, number and brightness, fluorescent proteins, multimerization, quantitative microscopy

Abbreviations

FFS, fluorescence fluctuation spectroscopy; FP, fluorescence protein; N&B, number and brightness; *pf*, fluorescence probability; PM, plasma membrane; PPI, protein-protein-interaction; sFCS, scanning fluorescence correlation spectroscopy

36 ## Introduction

37 A multitude of cellular processes, such as biomolecule transport, ion channel activity, cell-cell adhesion
38 and communication are regulated by protein-protein-interactions (PPIs) (1-3). "Classical" bulk biochemical
39 *in vitro* methods that are used to quantify PPIs (e.g., co-immunoprecipitation (co-IP), pull-down assays
40 and western blotting) cannot be used to obtain information about intracellular protein distribution in live-
41 cell samples or to monitor the effects of variations in concentrations between different cells (4, 5).
42 Conventional optical microscopy can visualize the localization of proteins, but its resolution is limited (4,
43 6). More complex approaches, such as fluorescence fluctuation spectroscopy (FFS), can assess the
44 interactions between molecules in complexes and obtain insights into cellular pathways and assembly
45 processes (4-8). FFS provides information about dynamics through the analysis of signal fluctuations from
46 fluorescently labeled molecules (6, 7, 9). Additionally, the magnitude of such fluctuations can be used to
47 derive quantitative information about the multimerization state (i.e., number of monomers in a multimer)
48 of the protein of interest (7-10).

49 A common strategy to investigate PPIs *in cellula* via FFS is the fusion of a fluorescent protein (FP) to the
50 protein of interest (7-9, 11). Comparison between the brightness of protein multimers tagged with FPs
51 and the brightness of a monomeric reference allows the quantification of FP monomers in the complex
52 and, thus, the oligomerization state of the protein of interest (5, 7, 12). A major problem for several FFS
53 applications that rely on FPs, though, is the presence of non-emitting "dark" proteins, which can be
54 quantified through the so-called fluorescence probability (*pf*) (7, 13). It is sometime assumed that FPs
55 have a *pf* value of 1 meaning that, for example, a trimer containing three FPs emits in average a three-
56 fold higher signal than a monomer labelled with one FP (5, 7). Instead, *pf* values of e.g. green emitting FPs
57 have been reported in the range between 0.5 and 0.8 (1, 2, 7, 13-19). Recently, we have systematically
58 quantified the *pf* of several FPs, focusing mainly on proteins emitting in the red part of the visible spectrum
59 (7). In summary, since high *pf* values are required for increased sensitivity, not all FPs are equally suitable

60 for oligomerization studies (7). Because of the presence of non-emitting FPs (i.e., *pf* lower than 1), FFS
61 approaches might underestimate the amount of FPs and therefore, the oligomeric state of the protein of
62 interest.

63 Some of the most used FPs are the green fluorescent protein (GFP) and its mutants, such as the
64 monomeric enhanced GFP (mEGFP) (5, 20). This FP has a high quantum yield (QY), enhanced
65 photostability, and minimal interference with the cellular machinery (20). Of note, several variants have
66 been engineered over the past few years (e.g. mNeonGreen (mNG), mGreenLantern (mGL), and Gamillus)
67 in an effort to optimize molecular brightness, folding efficiency, photostability, and pH stability of the
68 fluorescent probe (Table 1) (21-24).

69 **Table 1: Photophysical characteristics of the fluorescence proteins (FPs).** QY, Quantum yield; norm., normalized.

FP	λ_{ex} [nm]	λ_{em} [nm]	QY	Brightness*	cellular norm. <I>	pK_a	maturation [min]	Reference
mEGFP	488	507	0.71	38.0	1.0[#,†]	6.0	28.0	(21)
mNG	506	516	0.78	90.0	3.3[#]	5.7	18.0	(21)
mGL	503	514	0.72	74.0	6.3[#]	5.6	14.0	(21)
Gamillus	504	519	0.90	74.7	0.5[†]	3.4	8.0	(24)

70 * (extinction coefficient × QY)/1,000, where QY and extinction coefficients are measured at the absorbance peak (λ_{ex} ± 2 nm)
71 # Average intensity in FP-expressing BE (2)-M17 human neuroblastoma cells, relative to EGFP, using the P2A quantitative co-expression system
72 † Average intensity in FP-expressing HeLa cells, relative to EGFP

73

74 In the context of complex experiments in living cells, a FP might encounter different environments and pH
75 conditions (e.g. acidic pH in lysosomes, secretory granule and endosomes; neutral pH in the nucleus,
76 cytoplasm and endoplasmic reticulum (ER); basic pH in mitochondria and a pH gradient in the Golgi
77 network) (22, 25). Measurements of GFP at acidic pH have shown a decrease of the *pf* value, possibly due

78 to an increase of proteins in the dark-state (22, 26-28). Consequently, it would be useful to systematically
79 analyze the properties of the above-mentioned novel FPs, in order to perform an exact quantification of
80 PPIs, also in different intra-cellular environments.

81 Here, we benchmarked the performance of novel green FPs (mGL and Gamillus) against the well-
82 established mEGFP and mNG. The presence of non-fluorescent states and photostability under different
83 pH conditions was measured using Number & Brightness (N&B) and scanning fluorescence correlation
84 spectroscopy (sFCS) analysis (5). Our results indicate that some of the observed proteins are brighter,
85 although unstable under longer/stronger illumination. Furthermore, we identify which proteins are more
86 suitable for multimerization quantification, rather than "simple" imaging, also at different pH conditions.

87

88 # Materials and Methods

89 **Fluorescent protein constructs**

90 A detailed description of the cloning procedure of all constructs is available in the Supporting Information.
91 All plasmids generated for this work will be made available on Addgene (https://www.addgene.org/). A
92 schematic overview of the intracellular localization of the constructs is provided Fig S1A and an overview
93 of the linker sequences within the FP structures is provided in Table S1.

94 **Cell culture**

95 Human embryonic kidney cells from the 293T line (HEK293T, CRL-3216™) and Chinese hamster ovary cells
96 (CHO-K1, CCL-61™) were purchased from ATCC (Kielpin Lomianki, Poland). Both cell lines were cultured in
97 phenol red-free Dulbecco's modified Eagle's medium (DMEM) with 10% fetal bovine serum, 2 mM L-
98 glutamine, 100 U/mL penicillin, and 100 mg/mL streptomycin at 37 °C and 5% CO_2. Cells were passaged
99 every 2–3 days when they reached nearly 80% confluence in tissue culture flask, for 15 passages. All
100 solutions, buffers, and media used for cell culture were purchased from PAN-Biotech (Aidenbach,
101 Germany).

102 **Preparation for Microscopy Experiments**

103 For microscopy experiments, 6×10^5 (HEK293T) or 4×10^5 (CHO-K1) cells were seeded in 35 mm dishes
104 (CellVis, Mountain View, CA, USA) with optical glass bottom (#1.5 glass, 0.16–0.19 mm), 24 h before
105 transfection. HEK293T cells are preferred for sFCS measurements since they are relatively thick and
106 therefore suitable for sFCS based data acquisition perpendicular to the PM. CHO-K1 cells are rather flat
107 and characterized by a large cytoplasmic volume and therefore suitable for N&B measurements in the
108 cytoplasm. Cells were transfected 16–24 h prior to the experiment using 200 ng plasmid DNA per dish

109 with Turbofect (Thermo Fisher Scientific, Waltham, MA, USA) according to the manufacturer's
110 instructions.

111 For measurements under different pH conditions, the culture medium was exchanged with buffer
112 containing 140 mM NaCl, 2.5 mM KCl, 1.8 mM $CaCl_2$, 1.0 mM $MgCl_2$, and 20 mM HEPES with a pH value of
113 5.6, 7.4 or 9.2.

114 **Confocal microscopy system and setup calibration for fluorescence fluctuation spectroscopy**

115 All measurements were performed on a Zeiss LSM780 system (Carl Zeiss Microscopy GmbH, Oberkochen,
116 Germany) using a Plan-Apochromat 40×/1.2 Korr DIC M27 water immersion objective and a 32-channel
117 GaAsP detector array. Samples were excited with a 488 nm Argon laser and the fluorescence signal was
118 collected in a range of 498 to 606 nm in photon-counting mode after passing through a 488 nm dichroic
119 mirror. For the spectral analysis under different pH conditions, fluorescence was detected in spectral
120 channels of 8.9 nm width (23 channels between 491 nm and 690 nm). To decrease out-of-focus light, a
121 pinhole with size corresponding to one airy unit was used. All measurements were performed at 22 ± 1°C.

122 The confocal volume was calibrated daily by performing a series of point FCS measurements with Alexa
123 Fluor® 488 (AF488, Thermo Fischer, Waltham, MA, USA) dissolved in water at 30 nM, at the same laser
124 power and beam path used for N&B and sFCS measurements. Prior to that, the signal was optimized by
125 adjusting the collar ring of the objective and the pinhole position to the maximal count rate for AF488.
126 Then, five measurements at different locations were acquired, each consisting of 15 repetitions of 10 s,
127 and the data was fitted using a three-dimensional diffusion model including a triplet contribution. The
128 structure parameter S (defined as the ratio between the vertical and lateral dimension of the theoretical
129 confocal ellipsoid) was typically around 5 to 9, and the diffusion time τ_d around 30 to 35 µs.

130

131 **N&B measurements**

132 N&B analysis was performed as previously described (7, 10) with few modifications: 128x 128 pixel images
133 were acquired with pixel dimensions of 400 nm and a pixel dwell time of 50 µs. Image time-stacks of 105
134 scans were collected using the Zeiss Black ZEN software. The intensity time-stacks data were analyzed
135 using a custom Matlab code (The MathWorks, Natick, MA, USA). The Matlab algorithm utilizes the
136 equations from Digman *et al.* (11) for obtaining the molecular brightness and number as a function of
137 pixel position. Bleaching and minor cell movements are partially corrected using a boxcar-filter with an 8-
138 frame window applied pixel-wise, as previously described (7, 29, 30). Final brightness values were
139 calculated by extrapolating the partial brightness values (i.e., calculated within each 8-frame window) to
140 the earliest time point. Detector saturation leading to artefactual reduction in brightness was avoided by
141 excluding pixels with photon-counting rates exceeding 1 MHz. A schematic overview of the N&B analysis
142 is provided in Fig S1C.

143 **sFCS measurements**

144 Scanning FCS experiments were performed as previously described (7, 31), with a modified acquisition
145 mode. Briefly, a line scan of 256 × 1 pixels (pixel size ≈80 nm) were performed perpendicular to the
146 membrane with 472.73 µs scan time. Typically, 400,000 lines were acquired (total scan time ≈3 min) in
147 photon counting mode. Laser power values were typically between ≈1.5 µW (brightness analysis) and
148 ≈6 µW (photobleaching analysis). Scanning data were exported as TIFF files, imported and analyzed in
149 Matlab (The MathWorks, Natick, MA, USA) using a custom code as previously described (7, 31, 32). A
150 schematic overview of the sFCS analysis is provided in Fig S1D. Matlab custom-written code is available
151 from the corresponding author upon reasonable request.

152

153 **Brightness calibration and fluorophore maturation**

154 The molecular brightness, i.e. the photon count rate per molecule, is used as a measure for the oligomeric
155 state of protein complexes. This quantity is often based on the assumption that all fluorophores within an
156 oligomer are fluorescent. However, FPs can undergo dark state transitions or be in a non-mature, non-
157 fluorescent state (8). To quantify the amount of non-fluorescent FPs, we consider all these processes
158 together in a single parameter, the apparent fluorescence probability (*pf*), i.e. the probability of a FP to
159 emit a fluorescence signal. The determination of the *pf* value from apparent brightness values was
160 performed as previously described (7, 32). Shortly, for each sample and each experiment day, the average
161 brightness for a monomeric construct was determined from multiple cells (see e.g. Figs 2A and 3A). Then,
162 measurements were performed in several cells expressing the dimer constructs (Fig S2) and, from each of
163 these measurements and the average monomer brightness obtained before, one *pf* value was calculated
164 using the formula $p_f = {Brightness_{dimer}}/{Brightness_{monomer}} - 1$ (7, 32). The final *pf* value was
165 calculated as mean of such a set of measurements (see Figs 2B and 3B).

166 **Statistical analysis**

167 Data from at least three independent experiments were pooled and visualized using GraphPad Prism ver.
168 9.0.0 (GraphPad Software, LCC, San Diego, CA, USA). All resulting data were displayed as box plots with
169 single data points corresponding to measurements in single cells or as mean ± standard error of the mean
170 (SEM) plots. Median values and whiskers ranging from minimum to maximum values are displayed in the
171 box plots. The mean, median, interquartile range (IQR) are indicated in each graph together with the
172 sample size. Significance values are given in each graph and figure captions, respectively. Statistical
173 significance was tested by using D'Agostino-Pearson normality test followed by one-way ANOVA analysis
174 and the Tukey's or Fishers Least Significant Difference (LSD) multiple comparisons test.

175 # Results

176 **mGL and Gamillus are less photostable than mEGFP or mNG**

177 All monomeric FPs were evaluated for photostability at different laser powers using confocal microscopy,
178 in the context of a typical N&B experiment performed in CHO-K1 cells. Such an approach simply consists
179 of a time-series acquisition with continuous scanning over ca. two minutes. mGL and Gamillus displayed
180 higher photobleaching, both in the cytosol and at the PM, in comparison to mEGFP and mNG (Fig 1A and
181 1B, Table S2). For example, ≈30% of the total mGL was bleached after a ca. two-minute of continuous
182 scanning, using 2.4 µW excitation power. At the same time, N&B analysis provided the brightness of each
183 FP, as a function of the laser power. Although an accurate analysis should be performed at an excitation
184 power causing as low as possible bleaching (see next paragraph), Figs 1C and D confirm that the observed
185 brightness predictably increases roughly linearly with the laser power. As expected, due to the detection
186 geometry, a higher signal is observed for molecules restricted to the PM (33). Finally, Gamillus shows
187 generally a higher brightness, as especially noticeable for measurements at the PM or at higher excitation
188 powers.

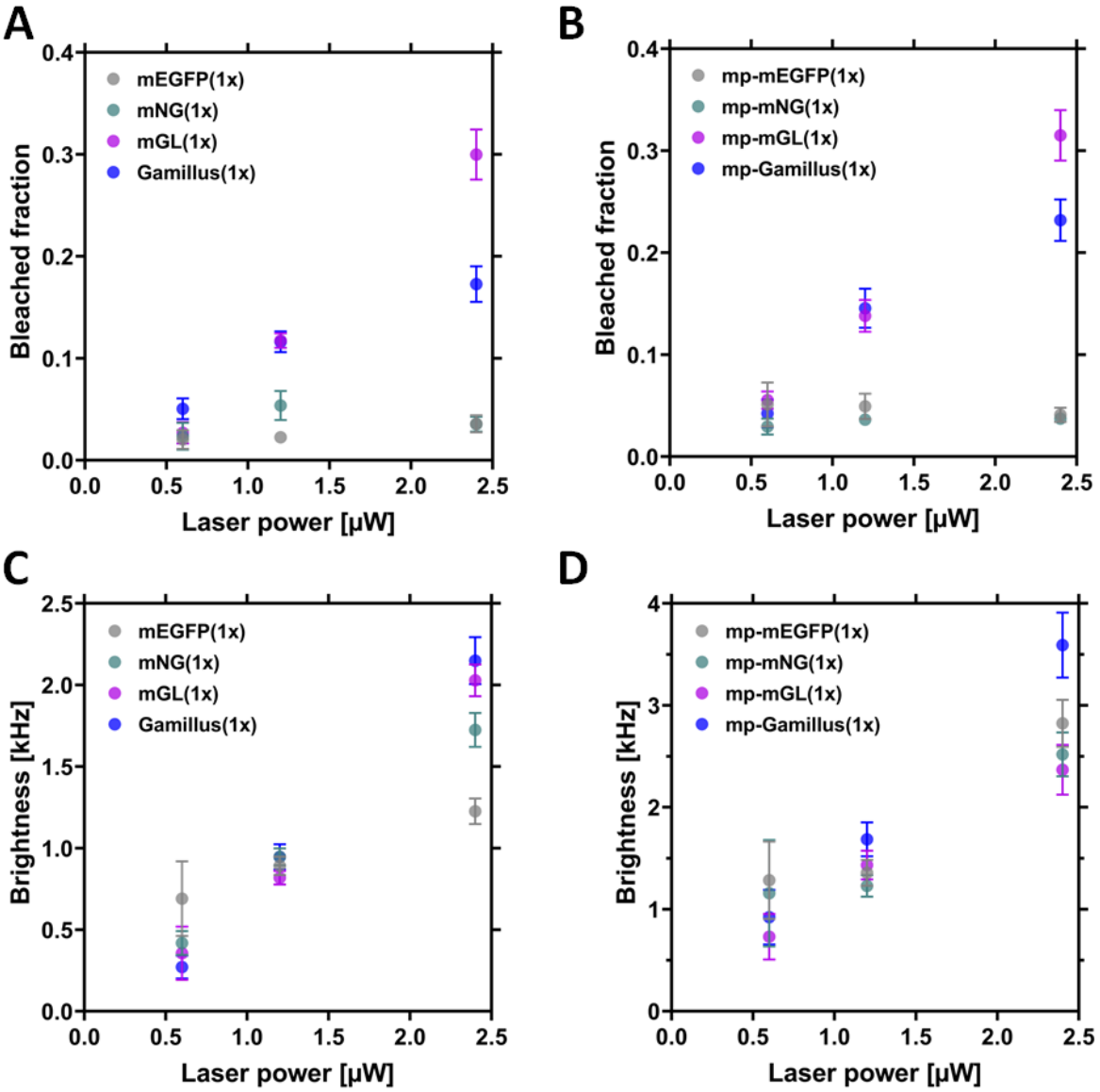

Fig 1: Comparison of the molecular brightness and bleached fraction for the monomeric FPs, as obtained from N&B measurements in CHO-K1 cells. CHO-K1 cells were transfected with plasmids coding for the monomeric cytosolic FPs (mEGFP(1x), mNeonGreen(1x) (here, called mNG(1x)), mGreenLantern(1x) (here called mGL(1x)) and Gamillus(1x)) or with membrane-anchored FPs. The latter are anchored to the inner leaflet of the PM via a myristoylated and palmitoylated (mp) peptide (mp-mEGFP(1x), mp-mNG(1x), mp-mGL(1x) or mp-Gamillus(1x)). N&B measurements were performed ≈16 h after transfection with a laser power of 0.6 µW, 1.2 µW and 2.4 µW. (A-B): Mean bleached fractions measured for cytosolic FPs (A) and for PM-anchored FPs (B), as a function of laser power. The bleached fraction indicates the amount of fluorescence signal lost after a N&B measurement. Error bars indicate the standard error of the mean (SEM). (C-D): Mean brightness values measured for cytosolic

198 FPs (C) and for PM-anchored FPs (D), as a function of laser power. Error bars represent the SEM. Exact values and sample sizes
199 are summarized in Table S2.

200

201 **Gamillus exhibits high brightness but low fluorescence probability**

202 To compare the brightness effectively observed in a typical confocal microscopy setup and, specifically, in
203 the context of FFS experiments, we have performed in-depth N&B analysis of FP monomer and dimer
204 constructs. In order to maintain bleaching below ≈15%, we have excited the fluorophores with a laser
205 power of 1.2 µW. CHO-K1 cells were transfected with the required plasmids and observed after 16 h. Fig
206 2A shows the brightness values measured for the different FP monomer constructs, either in the cytosol
207 or at the PM. The results follow, as expected, the general trend already described above (Figs 1C and D).
208 No significant difference can be observed between brightness values at this low laser power, with the
209 exception of mp-Gamillus displaying a higher brightness than the other membrane-associated constructs.

210 Next, we have performed similar experiments on dimer constructs of the same FPs (Fig S2A), in order to
211 calculate the *pf*, as shown in Fig 2B. All *pf* values are in the expected range, around 0.7, and no large
212 difference can be observed between the different fluorophores in general. Noticeably though, mp-
213 Gamillus exhibits *pf* values lower than those of the other FPs (in particular, significantly lower than mp-
214 mGL, ca. 0.6 vs. ca. 0.9).

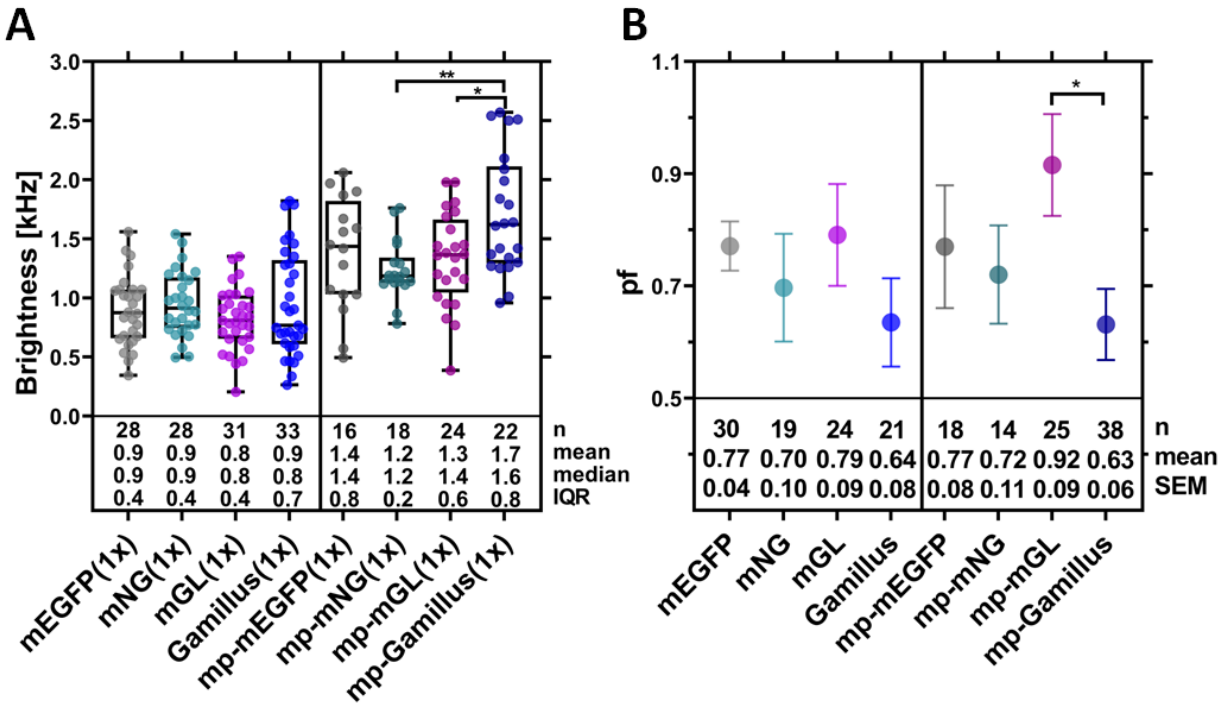

Fig 2: Comparison of brightness and fluorescence probability (*pf*) for the examined green FPs, as obtained from N&B measurements in CHO-K1 cells. N&B measurements were performed ≈16 h after transfection, using a laser power of 1.2 µW. (A): Box plot of the molecular brightness for the examined cytosolic and membrane-anchored FPs (i.e., mp-FP). Each point represents the average value measured in a single cells, from three independent experiments. Median values and whiskers ranging from minimum to maximum values are displayed. (B): Mean *pf* values calculated for the cytosolic and membrane-anchored FPs, using the brightness values measured for the corresponding FP dimers (Fig S2A). Data were collected from three independent experiments. The error bars represent the SEM. Sample size, mean/median, and interquartile range (IQR)/SEM are indicated below the graph. Statistical significance within both plots for selected sample pairs were determined using one-way ANOVA Tukey´s multiple comparison test (* $p < 0.05$, ** $p < 0.005$).

Performance comparison of FPs at different pH values

The fluorescence emission intensity of some FPs often decreases at low pH values due to protonation of the chromophore (22, 24, 26). Protonation can induce the transition to dark states and, therefore, negatively affect the accuracy of molecular brightness measurements (28). Here, the pH-dependent

229 fluorescence of the FPs was analyzed via confocal microscopy in the pH range from 5.6 to 9.2 in HEK293T
230 cells using constructs associated to the outer side of the PM via a glycosylphosphatidylinositol (GPI)
231 anchor. The fluorescence emission spectra of the different FPs did not change considerably in the assessed
232 pH range and no photoconversion was observed (Fig S3). Also, the photostability of the FP variants at
233 different pH conditions was qualitatively compared (Fig S4) using an excitation power of 6 µW, on a
234 specific position of the PM, for ca. three minutes. This configuration is usually employed for FCS
235 measurements at the PM and is different from the N&B whole-frame scanning approach used for the
236 experiments described in the previous paragraphs (10). GPI-mEGFP showed a good photostability at all
237 pH conditions, with the fluorescence signal decreasing by only ca. 20% (Figs S4A and S5). GPI-mNG(1x)
238 exhibited fast initial photobleaching, particularly at pH values 5.6 and 9.2, down to ca. 50% of the original
239 signal. At neutral pH, bleaching of GPI-mNG was only slightly higher than that of GPI-mEGFP (Figs S4B and
240 S5). A fast and substantial photobleaching, especially at neutral and low pH was observed for GPI-mGL
241 (Fig S4C and S5). Finally, as shown in Figs S4D and S5, a strong pH-dependency of photostability was
242 observed for GPI-Gamillus: at the highest pH the bleaching was minor (i.e., ca. 20%, similar to GPI-mEGFP),
243 while at neutral and low pH the emission signal dramatically decreased (i.e., to ca. 40% and 10% at pH 7.4
244 and 5.6, respectively). Overall, mEGFP showed the highest photostability for all pH conditions followed by
245 mNG and then Gamillus (pH < 9.2) and mGL, in agreement with the results from N&B analysis (Fig 1B).

246 Additionally, the molecular brightness of the different FPs under various pH conditions was evaluated for
247 monomer and dimer membrane-associated GPI-anchored constructs, and the corresponding *pf* values
248 were determined (Figs 3 and S2B). To complement the previous experiments, we used an alternative FFS
249 approach (i.e., sFCS (34)) and an alternative live-cell model (i.e., HEK293T) for this set of experiments. sFCS
250 experiments result in fluorescence auto-correlation curves which can be analyzed to extract parameters
251 such as diffusion coefficients of the labelled proteins, concentration and molecular brightness (see Fig S6
252 for representative examples). As shown in Fig 3A, the results obtained at pH 7.4 corroborate what was

253 observed also via N&B (Figs 1D and 2A), i.e. that Gamillus overall exhibits a higher brightness compared
254 to the other FPs. This observation holds true for all the tested pH conditions. In general, the observed
255 brightness values did not differ much among each other (being all within a ca. 15% variation interval) and
256 we did not observe an effect of pH, at least at the low laser powers used here.

257 More marked differences were observed, however, for the *pf* values. In general, this parameter showed
258 a negative correlation with increasing pH for GPI-mEGFP and a positive correlation for GPI-Gamillus. No
259 strong correlation was observed instead for GPI-mGL or GPI-mNG. At pH 5.6, the *pf* of GPI-Gamillus was
260 significantly lower than that of GPI-mEGP and, overall, the lowest among all investigated proteins. At
261 neutral pH, GPI-mGL showed the best performance, in agreement with what we observed for mp-mGL via
262 N&B (Fig 2B). At pH 9.2, no strong differences were observed in general among all FPs, although GPI-
263 Gamillus displayed by trend the highest *pf* value. Notably, we did not observe pH-induced changes in the
264 autocorrelation functions (indicating e.g. significant alterations in the triplet state fraction) for any FP, at

265 this low excitation power (Fig S6). An in-depth study of fluorescence intensity dynamics faster than ca. 1

266 ms would require, in general, approaches with higher temporal resolution.

267

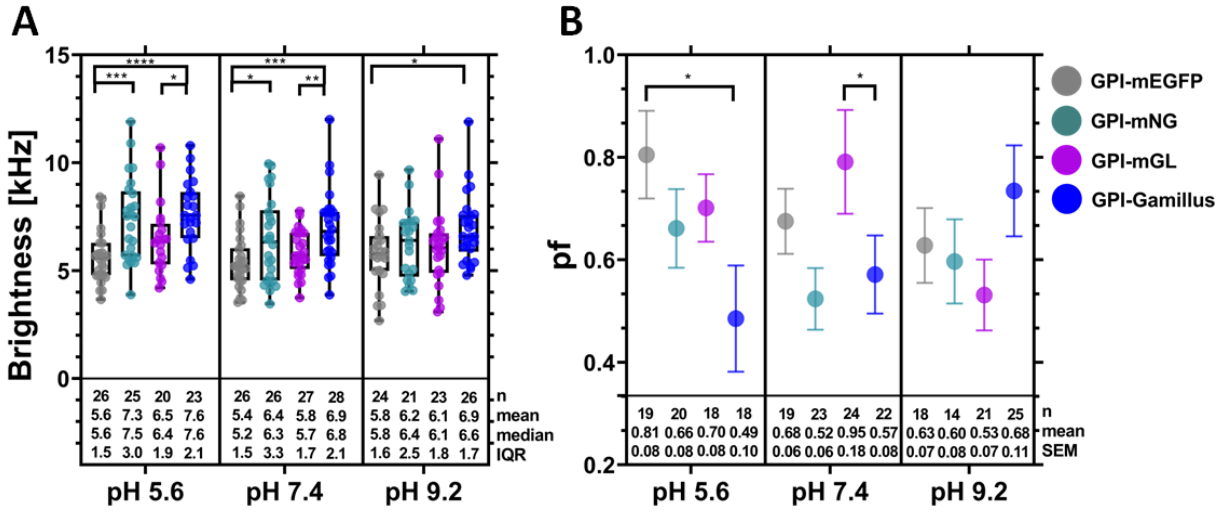

268

269 **Fig 3: Comparison of brightness and *pf* values for the examined FPs, as obtained from scanning fluorescence correlation**

270 **spectroscopy (sFCS) measurements in HEK293T cells, under different pH conditions (pH 5.6, pH 7.4, and pH 9.2).** sFCS

271 measurements were performed ≈16 h after transfection, using a laser power of 1.5 µW. (A): Box plots of the molecular brightness

272 for the membrane-anchored FPs GPI-mEGFP , GPI-mNG , GPI-mGL and GPI-Gamillus, for three different pH conditions. Each point

273 represents the average value measured in single cells, from three independent experiments. Median values and whiskers ranging

274 from minimum to maximum values are displayed. (B): Average *pf* values calculated using the brightness values measured for the

275 corresponding FP dimers (Fig S2B), for three different pH conditions. Data were collected from three independent experiments.

276 The error bars represent the SEM. Statistical significance was determined for selected sample pairs in both plots using one-way

277 ANOVA Fishers Least Significant Difference (LSD) multiple comparison test (* $p < 0.05$, ** $p < 0.005$, *** $p < 0.0005$, **** $p <$

278 0.0001).

279

280 ## Discussion

281 PPIs and, specifically, homo-multimerization can be quantified directly in living cells using quantitative
282 fluorescence microscopy approaches based on FFS (e.g., sFCS and N&B) (6-8). The molecular brightness
283 (i.e., photon count rate per molecule) derived from such experiments allows the determination of the
284 oligomeric state of FP-tagged protein complexes. (7, 8, 10). The reliability of such approaches is influenced
285 by the photophysical behavior of the FPs, which can be summed up by the *pf* parameter (7). The *pf* is
286 determined by the specific experimental conditions (e.g. excitation wavelength and power, duration of
287 illumination, geometry of the detection volume), sample environment (pH, ion composition, etc.),
288 intracellular biochemical processes (e.g. maturation time and folding efficiency) and photophysical
289 processes (photobleaching, quantum yield, triplet state formation, protonation- or light-induced
290 "blinking", long-lived dark states, etc.) (9, 20, 26-28, 34-40). Therefore, three requisites should be ideally
291 met by FPs used in typical FFS studies: i) high photostability, essential to allow time-based measurements
292 under continuous illumination, ii) high molecular brightness, required to achieve sufficient signal-to-noise
293 ratio to detect single molecule fluctuations and iii) a high *pf*, crucial for a large dynamic range and accuracy
294 of oligomerization measurements. In this study, we present a comprehensive analysis of novel GFP
295 variants (mGL and Gamillus) and their suitability for brightness-based oligomerization studies. Both
296 proteins were reported to mature remarkably quickly and to possess a high brightness and medium-low
297 acid sensitivity compared to mEGFP (see Table 1) (21, 24), thus suggesting that they are promising
298 candidates for quantitative FFS studies. These features are, at least partially, shared also by the
299 established GFP variant mNG (23), which is therefore also included in this study.

300 Previous studies have characterized these FPs and compared them to e.g. mEGFP as standard (see e.g.
301 (41)). Nevertheless, it must be noted that essential parameters, such as brightness, pH sensitivity or
302 photostability, are often measured with different methods and the outcome might depend on the specific
303 setup (23, 24, 41-43). Thus, it is reasonable to compare the FPs systematically using specific conditions

304 and approaches resembling those of actual FFS experiments. Following this logic, we used typical FFS
305 approaches (i.e., N&B and sFCS) to quantify the stability, brightness, pH sensitivity and *pf* of mEGFP, mNG,
306 Gamillus and mNG.

307 A first unexpected result is that, in general, we do not observe strikingly different brightness values
308 between each FP. While this observation can likely be explained by the distinctive experimental setup
309 (e.g. very low excitation power, longer acquisition times, specific intra-cellular localization (21, 42, 44)), it
310 is nevertheless relevant for users planning similar FFS-based investigations. Furthermore, the brightness
311 measured via FFS is an average value derived from a statistical analysis of single molecule fluctuations.
312 Such analysis is different from bulk methods that measure the fluorescence emission in a whole cell as a
313 readout of brightness. While remaining both valid, the different approaches might provide information
314 about different aspects of the fluorescent system. Finally, in our experimental conditions, Gamillus
315 displayed a higher brightness compared to the other FPs, at least when located at the PM or while using
316 higher laser powers. This observation was independently confirmed via both sFCS and N&B analysis.

317 Both techniques also indicate that the higher brightness of Gamillus is counterbalanced by a stronger
318 tendency to photobleach, at least in the conditions used in our experiments (e.g., pH 7.4). A similarly low
319 photostability was observed also for mGL, while mNG and mEGFP proved to be remarkably stable under
320 continuous irradiation. Of interest, the contrast with reports indicating a strong photostability of mGL and
321 Gamillus might be only apparent. A general comparison of these observations with previous studies is
322 complicated by the fact that, often, different conditions and experimental setups result in different
323 apparent photochemical behavior. For example, mEGFP was shown to be less stable than mNG under
324 widefield illumination, more stable under laser illumination (23) and similarly stable using a spinning disk
325 confocal microscope (42). Nevertheless, the photostability observed here at pH 7.4 for mEGFP is in the
326 same range as previously reported (23, 45). Also, mGL was reported to be less photostable than Clover

327 that, in turn, is less photostable than mEGFP (21, 45), in agreement with our observations. On the other
328 hand, in contrast to our observation, Shinoda *et al.* showed that Gamillus has a 2-fold higher photostability
329 than mEGFP under widefield illumination and acidic conditions (24). Once more, a possible explanation
330 for such discrepancies might reside in the considerably different experimental conditions which, in this
331 case, might be specifically relevant for FFS-based multimerization studies.

332 Next, we have measured the *pf* values for the different FPs, since this is a parameter of fundamental
333 importance for quantitative multimerization studies. Our results indicate that, in general, all the examined
334 FPs perform relatively well (i.e., *pf* ca. 0.7) and definitely better than most red or blue FPs (7, 19). In
335 particular, mGL excels in this context, with a *pf* value of 0.8 and above, as confirmed by both N&B and
336 sFCS in different cell models. This might be due to its fast maturation rate (21).

337 In the second part of our work, we compared the FPs under different pH conditions. This is relevant for
338 live-cell studies with FPs targeting e.g. acidic organelles, such as endosomes, secretory granules,
339 lysosomes, and Golgi-Network (pH range ca. 4.7-8 (46)), which play a role for the sorting, transport and
340 degradation of proteins (24, 25). In general, mNG and mGL did not exhibit a special sensitivity to changes
341 in pH values between 5.6 and 9.2. Neither of the monitored parameters (photostability, brightness or *pf*)
342 displayed a significant correlation with pH values.

343 In contrast, mEGFP showed an increase of *pf* at acidic pH, with this value being significantly higher than
344 that of Gamillus. We did not observe a strong decrease in mEGFP brightness at low pH values, as it was
345 instead previously reported (26, 28, 43, 44). This might be due to the low laser powers employed in our
346 studies, since a control experiment performed at a ca. four-fold higher laser power resulted in a decrease
347 in mEGFP brightness of ca. 40% (data not shown). Apart from light-induced photochemical effect, it might
348 also be possible that the data spread obtained at lower excitation power could partially mask a decrease

349 in brightness. In any case, our data show that the brightness of mEGFP at pH 5.6 is indeed slightly lower
350 than that of the other FPs.

351 Also Gamillus was influenced by changes in pH value. First, we observed that its brightness remained
352 higher than that of mEGFP, especially at low pH values. Interestingly, the photostability and the *pf*
353 decreased dramatically as a function of decreasing pH values. In contrast with the idea of Gamillus being
354 a FP particularly useful under acidic conditions (24), our data indicate that this fluorophore might perform
355 best in basic environments in the context of FFS measurements. It is possible that strong differences
356 between Gamillus and, e.g., mEGFP might be observed instead at pH values below those explored in this
357 work (i.e. pH <5.5).

358 In conclusion, our results indicate that, in general, mEGFP is a very good choice for the quantification of
359 multimerization via FFS, also at pH values between 5.6 and 7.4. Although its brightness is lower than other
360 examined FPs, its remarkable photostability would allow using higher excitation powers (thus increasing
361 its brightness). Bright FPs, such as Gamillus, could be efficiently used for e.g. qualitative imaging with short
362 acquisition times and low excitation powers. At neutral pH conditions, a remarkably high *pf* was observed
363 for mGL, although care should be taken in experiments in which photobleaching might represent an issue.
364 Finally, at basic pH conditions (e.g., up to 9.2), Gamillus represents an optimal choice based on a good
365 photostability, high *pf* and brightness.

366

367

Author Contribution

Research Planning, A.P., A.K.A. and S.C; Investigation, A.P. and A.K.A.; Data Analysis, A.P., A.K.A. and S.C.; Writing – Original Draft Preparation, A.P.; Writing – Review & Editing, A.K.A., V.D., and S.C.; Software, V.D., A.P. and S.C.; Supervision, S.C.

Acknowledgements

We thank all the members of the Physical Biochemistry group for useful feedback. VD is grateful for support by an HFSP long-term postdoctoral fellowship (HFSP LT0058/2022-L). This work was partially supported by the Deutsche Forschungsgemeinschaft (DFG) project number 407961559 to S.C.

376 ## References

377 1. Arant RJ, Ulbrich MH. Deciphering the subunit composition of multimeric proteins by counting
378 photobleaching steps. Chemphyschem. 2014;15(4):600-5.

379 2. Hillesheim LN, Chen Y, Müller JD. Dual-color photon counting histogram analysis of mRFP1 and
380 EGFP in living cells. Biophysical journal. 2006;91(11):4273-84.

381 3. Kuzmanov U, Emili A. Protein-protein interaction networks: probing disease mechanisms using
382 model systems. Genome Medicine. 2013;5(4):37.

383 4. Godin AG, Rappaz B, Potvin-Trottier L, Kennedy TE, De Koninck Y, Wiseman PW. Spatial Intensity
384 Distribution Analysis Reveals Abnormal Oligomerization of Proteins in Single Cells. Biophys J.
385 2015;109(4):710-21.

386 5. Petazzi RA, Aji AK, Chiantia S. Fluorescence microscopy methods for the study of protein
387 oligomerization. Prog Mol Biol Transl Sci. 2020;169:1-41.

388 6. Bacia K, Kim SA, Schwille P. Fluorescence cross-correlation spectroscopy in living cells. Nature
389 Methods. 2006;3(2):83-9.

390 7. Dunsing V, Luckner M, Zühlke B, Petazzi RA, Herrmann A, Chiantia S. Optimal fluorescent protein
391 tags for quantifying protein oligomerization in living cells. Sci Rep. 2018;8(1):10634.

392 8. Chen Y, Johnson J, Macdonald P, Wu B, Mueller JD. Observing protein interactions and their
393 stoichiometry in living cells by brightness analysis of fluorescence fluctuation experiments. Methods
394 Enzymol. 2010;472:345-63.

395 9. Chen Y, Wei LN, Müller JD. Probing protein oligomerization in living cells with fluorescence
396 fluctuation spectroscopy. Proc Natl Acad Sci U S A. 2003;100(26):15492-7.

397 10. Dunsing V, Chiantia S. A Fluorescence Fluctuation Spectroscopy Assay of Protein-Protein
398 Interactions at Cell-Cell Contacts. J Vis Exp. 2018(142).

399 11. Digman MA, Dalal R, Horwitz AF, Gratton E. Mapping the number of molecules and brightness in
400 the laser scanning microscope. Biophys J. 2008;94(6):2320-32.
401 12. Dunsing V, Petrich A, Chiantia S. Multicolor fluorescence fluctuation spectroscopy in living cells
402 via spectral detection. Elife. 2021;10.
403 13. Heesink G, Caron C, van Leijenhorst-Groener K, Molenaar R, Gadella TWJ, Claessens MMAE, et al.
404 Quantification of Dark Protein Populations in Fluorescent Proteins by Two-Color Coincidence Detection
405 and Nanophotonic Manipulation. The Journal of Physical Chemistry B. 2022.
406 14. Foo YH, Naredi-Rainer N, Lamb DC, Ahmed S, Wohland T. Factors affecting the quantification of
407 biomolecular interactions by fluorescence cross-correlation spectroscopy. Biophys J. 2012;102(5):1174-
408 83.
409 15. Liebsch F, Aurousseau MRP, Bethge T, McGuire H, Scolari S, Herrmann A, et al. Full-length cellular
410 β-secretase has a trimeric subunit stoichiometry, and its sulfur-rich transmembrane interaction site
411 modulates cytosolic copper compartmentalization. J Biol Chem. 2017;292(32):13258-70.
412 16. McGuire H, Aurousseau MR, Bowie D, Blunck R. Automating single subunit counting of membrane
413 proteins in mammalian cells. J Biol Chem. 2012;287(43):35912-21.
414 17. Ulbrich MH, Isacoff EY. Subunit counting in membrane-bound proteins. Nat Methods.
415 2007;4(4):319-21.
416 18. Wu B, Chen Y, Müller JD. Fluorescence fluctuation spectroscopy of mCherry in living cells. Biophys
417 J. 2009;96(6):2391-404.
418 19. Balasubramanian H, Sankaran J, Goh CJH, Wohland T. The dependence of EGFR oligomerization
419 on environment and structure: A camera-based N&B study. Biophysical Journal. 2022;121:4452-66.
420 20. Schwille P, Kummer S, Heikal AA, Moerner WE, Webb WW. Fluorescence correlation spectroscopy
421 reveals fast optical excitation-driven intramolecular dynamics of yellow fluorescent proteins. Proc Natl
422 Acad Sci U S A. 2000;97(1):151-6.

423 21. Campbell BC, Nabel EM, Murdock MH, Lao-Peregrin C, Tsoulfas P, Blackmore MG, et al.
424 mGreenLantern: a bright monomeric fluorescent protein with rapid expression and cell filling properties
425 for neuronal imaging. Proceedings of the National Academy of Sciences. 2020;117(48):30710.
426 22. Costantini LM, Baloban M, Markwardt ML, Rizzo M, Guo F, Verkhusha VV, et al. A palette of
427 fluorescent proteins optimized for diverse cellular environments. Nat Commun. 2015;6:7670.
428 23. Shaner NC, Lambert GG, Chammas A, Ni Y, Cranfill PJ, Baird MA, et al. A bright monomeric green
429 fluorescent protein derived from Branchiostoma lanceolatum. Nat Methods. 2013;10(5):407-9.
430 24. Shinoda H, Ma Y, Nakashima R, Sakurai K, Matsuda T, Nagai T. Acid-Tolerant Monomeric GFP from
431 Olindias formosa. Cell Chemical Biology. 2018;25(3):330-8.e7.
432 25. Casey JR, Grinstein S, Orlowski J. Sensors and regulators of intracellular pH. Nat Rev Mol Cell Biol.
433 2010;11(1):50-61.
434 26. Haupts U, Maiti S, Schwille P, Webb WW. Dynamics of fluorescence fluctuations in green
435 fluorescent protein observed by fluorescence correlation spectroscopy. Proc Natl Acad Sci U S A.
436 1998;95(23):13573-8.
437 27. Widengren J, Mets Ü, Rigler R. Photodynamic properties of green fluorescent proteins
438 investigated by fluorescence correlation spectroscopy. Chemical Physics. 1999;250(2):171-86.
439 28. Vámosi G, Mücke N, Müller G, Krieger JW, Curth U, Langowski J, et al. EGFP oligomers as natural
440 fluorescence and hydrodynamic standards. Sci Rep. 2016;6:33022.
441 29. Dunsing V, Mayer M, Liebsch F, Multhaup G, Chiantia S. Direct evidence of amyloid precursor-like
442 protein 1 trans interactions in cell-cell adhesion platforms investigated via fluorescence fluctuation
443 spectroscopy. Mol Biol Cell. 2017;28(25):3609-20.
444 30. Sperber HS, Welke RW, Petazzi RA, Bergmann R, Schade M, Shai Y, et al. Self-association and
445 subcellular localization of Puumala hantavirus envelope proteins. Sci Rep. 2019;9(1):707.

446 31. Tzoneva R, Stoyanova T, Petrich A, Popova D, Uzunova V, Momchilova A, et al. Effect of Erufosine
447 on Membrane Lipid Order in Breast Cancer Cell Models. Biomolecules. 2020;10(5).
448 32. Petrich A, Dunsing V, Bobone S, Chiantia S. Influenza A M2 recruits M1 to the plasma membrane:
449 A fluorescence fluctuation microscopy study. Biophys J. 2021;120(24):5478-90.
450 33. Smith EM, Macdonald PJ, Chen Y, Mueller JD. Quantifying protein-protein interactions of
451 peripheral membrane proteins by fluorescence brightness analysis. Biophys J. 2014;107(1):66-75.
452 34. Ries J, Schwille P. Studying slow membrane dynamics with continuous wave scanning fluorescence
453 correlation spectroscopy. Biophys J. 2006;91(5):1915-24.
454 35. Balleza E, Kim JM, Cluzel P. Systematic characterization of maturation time of fluorescent proteins
455 in living cells. Nat Methods. 2018;15(1):47-51.
456 36. Hendrix J, Flors C, Dedecker P, Hofkens J, Engelborghs Y. Dark states in monomeric red fluorescent
457 proteins studied by fluorescence correlation and single molecule spectroscopy. Biophys J.
458 2008;94(10):4103-13.
459 37. Hur KH, Macdonald PJ, Berk S, Angert CI, Chen Y, Mueller JD. Quantitative measurement of
460 brightness from living cells in the presence of photodepletion. PLoS One. 2014;9(5):e97440.
461 38. Ries J, Chiantia S, Schwille P. Accurate determination of membrane dynamics with line-scan FCS.
462 Biophysical journal. 2009;96(5):1999-2008.
463 39. Schenk A, Ivanchenko S, Röcker C, Wiedenmann J, Nienhaus GU. Photodynamics of red
464 fluorescent proteins studied by fluorescence correlation spectroscopy. Biophys J. 2004;86(1 Pt 1):384-94.
465 40. Shaner NC, Steinbach PA, Tsien RY. A guide to choosing fluorescent proteins. Nat Methods.
466 2005;2(12):905-9.
467 41. Cranfill PJ, Sell BR, Baird MA, Allen JR, Lavagnino Z, de Gruiter HM, et al. Quantitative assessment
468 of fluorescent proteins. Nat Methods. 2016;13(7):557-62.

469 42. Heppert JK, Dickinson DJ, Pani AM, Higgins CD, Steward A, Ahringer J, et al. Comparative
470 assessment of fluorescent proteins for in vivo imaging in an animal model system. Mol Biol Cell.
471 2016;27(22):3385-94.
472 43. Liu Y, Kim HR, Heikal AA. Structural basis of fluorescence fluctuation dynamics of green fluorescent
473 proteins in acidic environments. J Phys Chem B. 2006;110(47):24138-46.
474 44. Steiert F, Petrov EP, Schultz P, Schwille P, Weidemann T. Photophysical Behavior of mNeonGreen,
475 an Evolutionarily Distant Green Fluorescent Protein. Biophys J. 2018;114(10):2419-31.
476 45. Lam AJ, St-Pierre F, Gong Y, Marshall JD, Cranfill PJ, Baird MA, et al. Improving FRET dynamic range
477 with bright green and red fluorescent proteins. Nat Methods. 2012;9(10):1005-12.
478 46. Theillet FX, Binolfi A, Frembgen-Kesner T, Hingorani K, Sarkar M, Kyne C, et al. Physicochemical
479 properties of cells and their effects on intrinsically disordered proteins (IDPs). Chem Rev.
480 2014;114(13):6661-714.

481

482

483 ## Supporting Information

484 Supporting Materials and Methods

485 **Table S1: Overview of the linker sequences of the homo-dimers for the different fluorescence protein**
486 **(FP) constructs used in this study.** mp: myristoylated and palmitoylated peptide, GPI:
487 glycosylphosphatidylinositol anchor.

488 **Table S2: Overview of molecular brightness and bleached fraction values measured via number and**
489 **brightness (N&B) analysis for all FPs in the cytosol and at the plasma membrane (PM).** Data correspond
490 to Fig 1 of the main manuscript.

491 **Fig S1: Schematic overview of the experimental setup.** (A) Overview of the different fluorescent proteins
492 (FPs) used in this study: cytosolic/soluble FPs, membrane associated constructs with the myristoylated
493 and palmitoylated (mp) peptide and glycosylphosphatidylinositol (GPI)-anchor linked to the FP as a
494 monomer or homo-dimer. The FPs used in this study were mEGFP, mNeonGreen (mNG), mGreenLantern
495 (mGL) and Gamillus. (B) Overview of the experimental procedure. One day after seeding, cells are
496 transfected. On the day after, cells are directly used for Number and Brightness (N&B) measurements or
497 are washed and equilibrated in HEPES-Buffer with the appropriate pH before each measurement for
498 scanning fluorescence correlation spectroscopy (sFCS) and spectral analysis. (C) N&B acquisition results in
499 a three-dimensional (x-y-time) image stack. A ROI is selected around a cell or membrane region. Then,
500 brightness (ε) values are calculated in each pixel. The results are then visualized as average intensity (<I>)
501 and average brightness (<ε>) map and histogram. (D) sFCS measurements are performed perpendicular
502 to the plasma membrane (PM), as also shown in panel (B). Scan lines (represented as kymographs) are

503 aligned and intensity at PM is integrated. Then, the brightness and the ACF are calculated from the
504 intensity trace and the ACF is analysed with a two-dimensional diffusion model.

505 **Fig S2: Brightness comparison for different green FP homo-dimers.** (A): N&B measurements were
506 performed ≈16 h after transfection in CHO-K1 cells, using a laser power of 1.2 µW. Box plot of the
507 molecular brightness in kHz for the examined cytosolic and membrane-anchored FP (i.e., mp-FP) homo-
508 dimers. Each point represents the average value measured in a single cell, pooled from three independent
509 experiments. (B): sFCS measurements were performed in HEK293T cells for different pH conditions (pH
510 5.6, pH 7.4, and pH 9.2) ≈16 h after transfection, with a laser power of 1.5 µW. Box plots with single data
511 points from three independent experiments show the molecular brightness in kHz for the homo-dimers
512 of GPI-mEGFP , GPI-mNG , GPI-mGL and GPI-Gamillus. Median values and whiskers ranging from minimum
513 to maximum values are displayed. Sample size, mean, median, and interquartile range (IQR) are indicated
514 in the graph. Statistical significance was determined for both plots using one-way ANOVA Tukey´s multiple
515 comparison test; * $p < 0.05$, ** $p < 0.005$, ***$p < 0.0005$, ****$p < 0.0001$.

516 **Fig S3: Normalized FP emission spectra at different pH values.** Average emission spectra of GPI-mEGFP
517 (A), GPI-mNG (B), GPI-mGL (C), and GPI-Gamillus (D) measured via spectral imaging (23 spectral channels
518 from 491 nm to 695 nm) using 488 nm excitation on HEK 293T cells supplemented with buffer at different
519 pH values (5.6, 7.4 and 9.2). At each pH value, ca. 10 cells were imaged, acquiring ten frames. To obtain
520 the average emission spectra, pixels corresponding to the PM were semi-manually segmented (manual
521 selection followed by removal of pixels with intensities below 25% of the maximum pixel intensity in the
522 selected region) and detected spectra averaged over all pixels and cells measured at each pH.

523 **Fig S4: Comparison of photostability for different monomeric green FPs under different pH conditions**
524 **via sFCS measurements.** HEK293T cells were transfected with the appropriate FP construct, washed on
525 the next day with HEPES buffer with the corresponding pH (pH 5.2 (magenta), pH 7.4 (green), and pH 9.2

526 (blue)) and then measured with a laser power of 6 µW, which is 4-fold higher than that used for standard
527 sFCS measurements. The emission intensities were normalized to the initial values. Representative
528 photobleaching curves are shown for GPI-mEGFP (A), GPI-mNG (B), GPI-mGL (C) and GPI-Gamillus (D).
529 Solid line represents a double exponential fit, as guide to the eye.

530 **Fig S5: Comparison of bleached fractions for the examined monomeric FPs, at different pH values**. The
531 decrease of the fluorescence signal has been quantified after a 180 s sFCS measurement, as exemplified
532 in Fig S4. For each FP, between 13 and 15 measurements from 3 independent samples were performed.
533 Statistical significance was determined using one-way ANOVA Tukey´s multiple comparison test; * $p <$
534 0.05, ** $p < 0.005$, ***$p < 0.0005$. Different symbols refer to comparisons to GPI-mEGFP (*), GPI-mNG (#),
535 GPI-mGL (†).

536 **Fig S6: Representative sFCS autocorrelation functions and fit curves obtained for cells expressing GPI-**
537 **FPs, under different pH conditions.** Fit curves (solid line) were obtained by fitting a two-dimensional
538 diffusion model to the data, as described in the main text (Methods section).

539